Estimation of the air shower depth of the maximum development by the relative fraction of muons and the composition of cosmic rays in the energy region $E_0 \geq 5$ EeV by Yakutsk array data

S. P. Knurenko[*] and I. S. Petrov[†]

Yu.G. Shafer Institute of Cosmophysical Research and Aeronomy, Yakutsk, Russia

The paper presents joint analysis of the characteristics of the electron-photon and Cherenkov components, and muons with a threshold $\varepsilon_{\text{thr}} \geq 1$ GeV and zenith angles less than 60°. The analysis is based on complex data of air shower registration. A quantitative estimation of muons at different distances from the shower axis and the ratio of muons and charged particles at a distance of 600 m are obtained. The empirical relationship found between $\rho_\mu(600)/\rho_{\mu+e}(600)$ and the depth of the maximum X_{max} estimated by Cherenkov light data. It allowed to estimate X_{max} in individual showers by fraction of muons $\rho_\mu(600)/\rho_{\mu+e}(600)$. From the set of such showers, the dependence of X_{max} on the energy E_0 was found. Mass composition of cosmic rays with highest energies is estimated by comparison of the experimental X_{max} and QGSJetII-04 simulation X_{max} for different primary nuclei. The composition of cosmic rays determined from the muon component of air showers, mainly consists of protons and helium nuclei in the energy range 5–10 EeV. At energies greater than 30 EeV the mass composition is becoming heavier due to CNO and iron nuclei.

I. INTRODUCTION

At present, cosmic rays have been measured up to energies of ~300 EeV. Very little is known about the physical properties of particles of such high energies; the mechanisms of their generation and acceleration in sources and outer space are unknown [1–5]. According to recent observations, possible cosmic ray sources in this energy range are cosmic bubble structures [6], supernova remnants, compact jets of active galactic nuclei [7], galaxy clusters [8], radio galaxies [9], and gamma-ray bursts [10]. Hypotheses about particles of similar energies and their possible sources were expressed in works [11,12].

The properties of these particles are being studied at large air shower experiments in the Yakutsk [13], Auger [14], and Telescope Array [15,16]. One of the main directions in these studies is to obtain information on the atomic weight of the primary particles [17–19].

The mass composition of cosmic rays has only been directly measured up to energies of 100 TeV in experiments on satellites and balloons [20–27]. For higher energies, the mass composition is studied indirectly by air shower methods, analyzing the longitudinal development of individual showers [28–31] and the integral characteristics of showers at sea level [32–35]. The results obtained indirectly largely depend on the experimental equipment, the atmospheric conditions, the experimental data processing techniques, the model of hadronic interactions, and other factors. Therefore, to verify the previously obtained results on mass composition, it is important to obtain the same information by a different method and different air shower component, for example, radio emission [36,37] and muons.

It is known that the muon component is sensitive to the mass composition of the primary particles producing the air shower [32,38–41], as can be seen by calculations based on the QGSjetII-04 model for the primary proton and iron nucleus. Calculations have shown that a joint analysis of muons with the longitudinal development of air showers is able to provide a reliable estimation of the mass composition of cosmic rays. With higher-accuracy measurements, it is possible to separate the primary particles types that produce air showers according to their atomic weight [32,34].

For 50 years the Yakutsk array has been registering air showers of ultrahigh energies ~$E_0 \geq 0.1$ EeV. The exposure of the Yakutsk array for 40 years is 5520 km$^2 \cdot$ sr $\cdot$ year. During this time, unique data have been collected on showers measuring the electron-photon and muon components, as well as the Cherenkov and radio components of the air shower. Table I shows, as an example, part of the data for 2009–2016. Table I shows the observation time, the number of registered air showers, the ratio of analyzed showers, the number of showers with muon components, the number of showers with Cherenkov component, and the number of

[*]knurenko@ikfia.ysn.ru
[†]Corresponding author.
igor.petrov@ikfia.ysn.ru

TABLE I. Air shower statistics registered at the Yakutsk array. Year (period of observations), T (time of observations in hours), N (number of air showers registered), Data processed [percentage of analyzed data (%)], N_μ (number of air showers registered by muon detectors), N_{Ch} (number of air showers registered by Cherenkov light detectors), T_{Ch} (time of observations with Cherenkov light detectors), E ≥ 10 EeV (number of air showers with energy greater than 10 EeV), $S \cdot T \cdot \Omega$ (exposure of the Yakutsk array in $km^2 \cdot sr \cdot h$).

Year	T	N	Data processed (%)	N_μ	N_{Ch}	T_{Ch}	E ≥ 10 EeV	$S \cdot T \cdot \Omega$
09–10	6154	113138	87	60618	9897	622	10	6.89×10^5
10–11	6455	137830	89	56130	8611	508	15	7.23×10^5
11–12	6534	155351	91	54559	9227	482	15	7.31×10^5
12–13	6515	149381	92	89430	10219	592	17	7.29×10^5
13–14	6446	147589	91	72110	7164	396	15	7.22×10^5
14–15	6365	140101	72	82392	7838	429	15	7.13×10^5
15–16	5671	127490	82	62599	4819	314	11	6.35×10^5

showers with energies greater than 10 EeV. During 50 years of continuous observations at the Yakutsk array, 2.7 million showers with a muon component and energies greater than 50 PeV were registered. In the present work, air showers of the highest energies with $E_0 \geq 5$ EeV are considered.

II. EXPERIMENTAL DATA OF AIR SHOWER MUON COMPONENTS: COMPARISON WITH CALCULATIONS

The cascade process of muon production in the atmosphere depends on the point of the first interaction of the primary nucleus with atoms of and ionization losses per unit path of the particle. For a heavy nucleus, the point of the first interaction is going to be higher in the atmosphere than for a light nucleus. Thus, the air shower is developing earlier and the shower development maximum X_{max} is going to be higher in the atmosphere. Due to the difference in the absorption paths of the muon and electron-photon components at sea level, the fraction of muons $\rho_\mu(600)/\rho_{\mu+e}(600)$ is larger for heavy nuclei and less for light nuclei. As shown in [32], showers produced by protons and iron nuclei are concentrated at different levels of X_{max}; therefore, the most sensitive parameter to X_{max}—and to mass composition—is going to be the fraction of muons $\rho_\mu(600)/\rho_{\mu+e}(600)$ which is the ratio of the muon flux density ρ_μ to the flux density of charged particles $\rho_{\mu+e}$ (which for this work was taken at a distance of 600 m from the air shower axis).

To measure the muon flux with a threshold $\varepsilon_{thr} \geq 1$ GeV, we used standard scintillation detectors of the Yakutsk array [42] (Fig. 1). Standard scintillation detectors have an area of s = 2 m^2 and a threshold $\varepsilon_{thr} \geq 10$ MeV. In the center of the array there are additional scintillation detectors with an area of s = 1 m^2 and a threshold $\varepsilon_{thr} \geq 1.8$ MeV. A standard detector consists of nine blocks with s = 0.25 m^2 each. Scintillators have special painted rings to eliminate the radial dependency of the charged particles hitting the detector.

The detectors were placed in underground galleries, under a layer of soil 500 $g \cdot cm^{-2}$ thick. Three detectors with area s = 16 m^2 each were located at distances of 300 m and 500 m from the center of the array. Three detectors with an area of 20 m^2 each were located at distances of 500 m and 800 m. A large muon detector with s = 190 m^2 was located at a distance of 150 m from the center of the array. Figure 2 shows one the underground muon station with ten scintillation detectors with an area of 2 m^2 each. Registration of muon signals are carried out by separate Analog-to-digital converter with buffer and subsequent recording of the signal to the memory when the received trigger signal is sent to the central station.

In measurements of muons, we also used three muon telescopes with an area of 2 m^2 each (Fig. 3). These telescopes are part of the Obscura stations, which register differential fluxes of Cherenkov light, charged particles, and muons. The Obscura stations are located at distances of 300 m, 350 m, and 500 m from the center of the array (Fig. 4).

All ground based scintillation and underground muon detectors are shown on the scheme of the Yakutsk array (Fig. 4). The subfigure shows the central part of the Yakutsk array, on the basis of which the Small Cherenkov array was created for the registration of air showers with energies of 10^{15}–10^{17} eV, including the registration of the shower cascade curve by the Obscura stations [43,44]. The Small Cherenkov array has its own trigger, which is synchronized with the trigger of the main array via the GPS. All information about the registered showers is stored locally in the stations of the Small Cherenkov array. Then, if there is, a trigger signal from the Small Cherenkov array the data is written to the database. For quick viewing of the signal, it can be displayed on the screen and analyzed. An example of simultaneous measurement of a charged component (electrons and muons) and muons with a threshold $\varepsilon_{thr} \geq 1$ GeV by a muon telescope is shown in Fig. 5.

Signals are registered at the distance R = 350 m from air showers axis by a ground [Fig. 5(a)] and underground detectors (Fig. 5). As one can see in Fig. 5(a) there are two
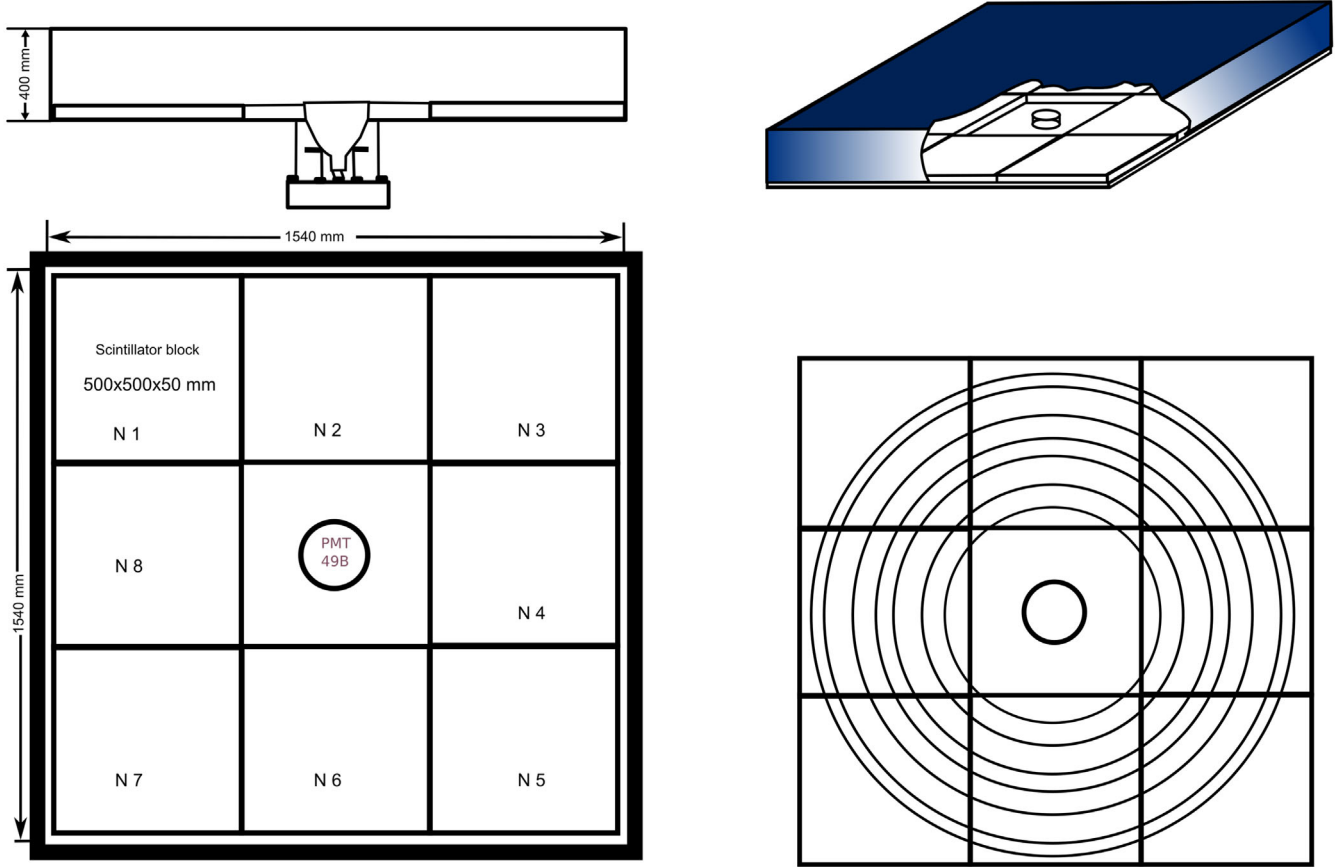
FIG. 1.   Standard scintillation detector with area $s = 2$ m^2, threshold $\varepsilon_{thr} \geq 10$ MeV at the Yakutsk array.

pulses—the first one is narrower and is generated by muons and the second one is generated by electrons, since there is no trace of it in Fig 5(b).

A. Ultrahigh energy showers selection

For the analysis of the muon component, 802 air shower events with energies $E_0 \geq 5$ EeV and zenith angles $\theta \leq 60°$

FIG. 2.   Muon detector with total area of 20 m^2 for registering muons with a threshold $\varepsilon_{thr} \geq 1$ GeV.
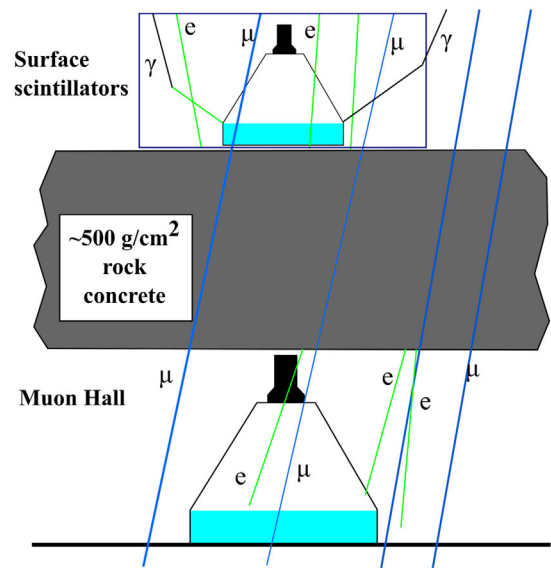

FIG. 3.   Scheme of the muon telescope used in the Obscura stations. The telescope is two scintillation detectors mounted on top of each other and separated by concrete.
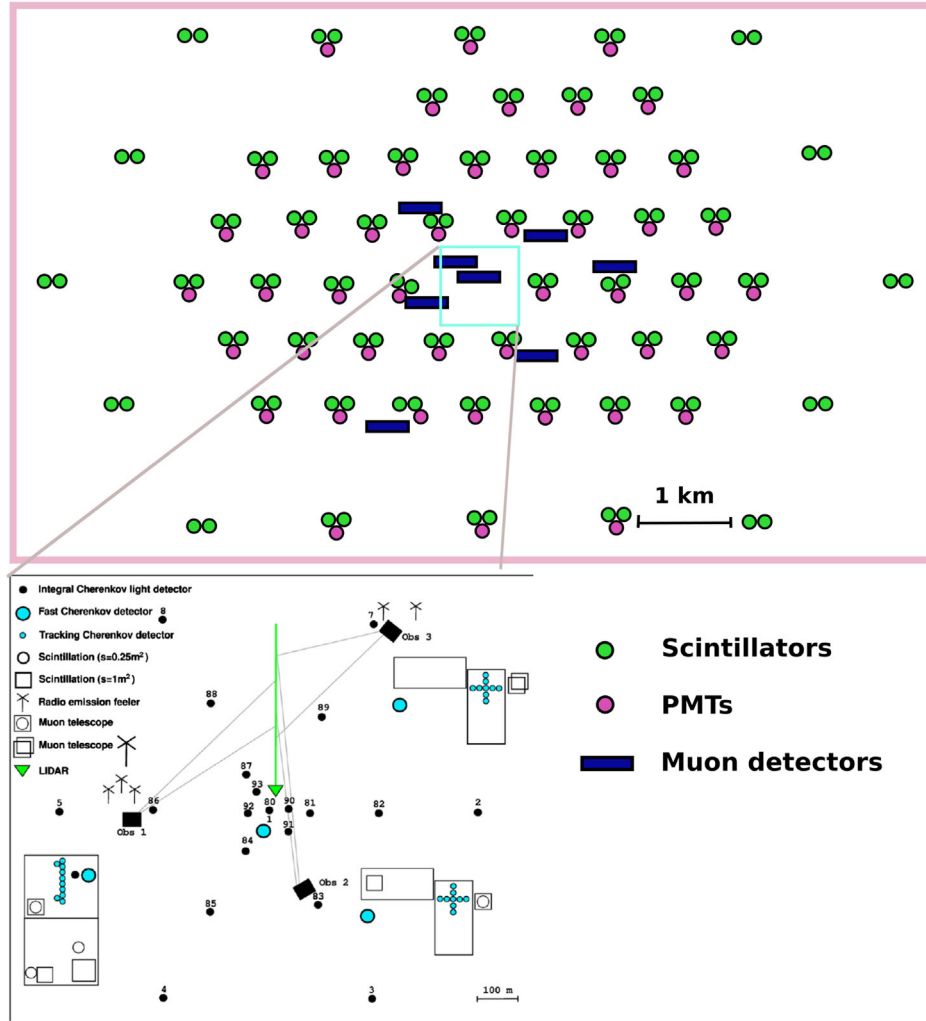
FIG. 4. Layout of observation stations at the Yakutsk array. Double dots represent stations on the setup, each station has two scintillation detectors, triple dots represent stations with Cherenkov detectors, rectangles represent muon detectors. Separately, the central part of the Yakutsk array is taken out, where the Small Cherenkov array is located.

were selected. In addition we used following criteria: the shower axis had to be within a circle with a radius of 1200 m from the center of the array; muon measurements in the distance range 200–1000 m; the accuracy of determining the axis was 10–20 m along the X_0 axis, and 15–25 m along the Y_0 axis. The accuracy of determining $\rho_\mu(600)/\rho_{\mu+e}(600)$ should have been ~10–15%.

The accuracy of $A = \rho_\mu(600)/\rho_{\mu+e}$ was determined by following method. First, we empirically established (in the course of analyzing the operation of adjacent scintillation detectors) total measurement accuracy of muon flux density, i.e., instrumental (statistical) and systematic, which is related to absolute calibration of scintillation detectors [45]. In our case total uncertainty of measurements of the muon flux density is expressed as [46,47]

$$D_\mu = \sigma^2(\rho_\mu(600))^2$$
$$= (\rho_\mu(600))^2 \cdot \left(\beta^2 + \frac{1+\alpha^2}{s \cdot \rho_\mu(600) \cdot \cos\theta}\right), \quad (1)$$

where β^2 is the relative measurement error which ensures the accuracy of the instrumental variance of the detector response, and α^2 is the Poisson statistical error,

$$\sigma(A) = \frac{\partial}{\partial\rho_\mu(600)} A \cdot \sigma(\rho_\mu(600)) = \frac{\sigma(\rho_\mu(600))}{\rho_{\mu+e}(600)}. \quad (2)$$

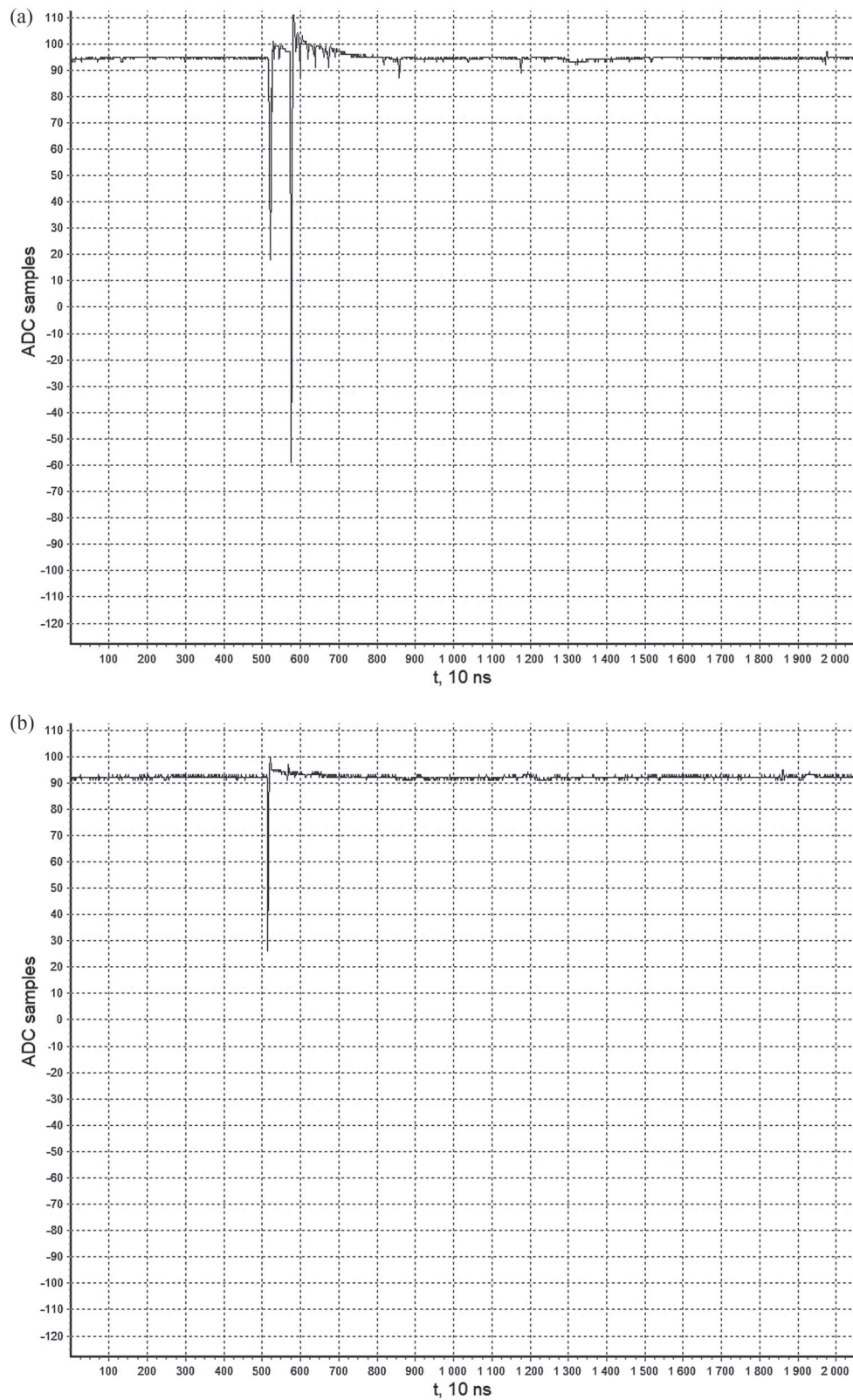In order to separate instrumental and systematic errors we will square (2)

FIG. 5.   Signals from scintillation detectors: ground (a) and underground (b).
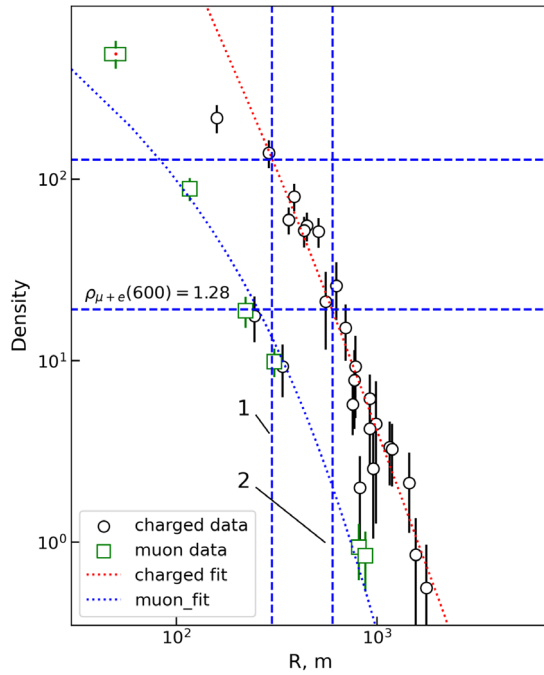
FIG. 6. Individual shower 05.01.18. $E_0 = 20.9 \pm 4.2$ EeV and the zenith angle is $44.8 \pm 1.2°$. Fraction of muons at the distance of 600 m from the shower axis $\rho_\mu(600)/\rho_{\mu+e}(600) = 0.107$. (1) $\rho_{\mu+e}(300)$ flux density of charged particles and muons at the distance of 300 m from the air shower. (2) $\rho_{\mu+e}(600)$ flux density of charged particles and muons at the distance of 600 m from the air shower.

$$D_A = \sigma^2(A) = \frac{\sigma^2(\rho_\mu(600))}{\rho_{\mu+e}^2(600)}$$

$$= \frac{1}{\rho_{\mu+e}^2(600)} \cdot \left(\beta^2 + \frac{1+\alpha^2}{s \cdot \rho_\mu(600) \cdot \cos\theta} \right), \quad (3)$$

with systematic error,

$$D_A^{\text{sys}} = \frac{\beta^2}{\rho_{\mu+e}^2(600)}. \quad (4)$$

which allows us to estimate statistical and systematic errors. In our case the statistical error is equal to ~5%, and the systematic error is ~15%, with total error equal to ~16%.

With these criteria, selected air showers had approximately similar conditions for the registration and close measurement accuracy of the main characteristics of air showers; there were 643 air shower events satisfying criteria. In each shower, the classification parameters $\rho_\mu(600)/\rho_{\mu+e}(600)$ were determined from the measured flux of charged particles and muons. An example of one of the showers is shown in Fig. 6. The energy of this shower is 20.9 ± 4.2 EeV, and the zenith angle is $44.8 \pm 1.2°$. This particular air shower has been registered by six different

muon detectors—represented by squares—in the distance range 200–1000 m. Experimental data is fitted by Eq. (5) and represented by blue dotted line. Using classification parameter ρ_μ and $\rho_{\mu+e}$, muon and charged flux densities at the distance 600 m, we determined the fraction of muons $\rho_\mu(600)/\rho_{\mu+e}(600)$.

$$f(R) = \rho_\mu(600) \cdot \left(\frac{R}{600} \right)^{-0.75} \cdot \left(\frac{R+280}{880} \right)^{0.75-b}$$

$$\cdot \left(\frac{R+2000}{2600} \right)^{-6.5}, \quad (5)$$

where b is the slope parameter.

The air shower energy E_0 is estimated by measured muon-flux density ρ_μ according to Eq. (6) [32]

$$\log_{10} E_0 = 18.33 + 1.12 \cdot \log_{10} \rho_\mu(R = 600, \theta). \quad (6)$$

There is a good agreement between the energy estimated from muons and the method adopted at the Yakutsk experiment for estimating the energy from the parameter $\rho_{\mu+e}(600)$. The result of comparing the shower energy estimations by two methods is given in Ref. [32]. As follows from this work, the agreement between two estimations is within an accuracy of 5% (Fig. 7).

B. Air shower depth of maximum by muon component

We selected individual air showers with measured Cherenkov light, charged and muon component data. We reconstructed X_{max} (the depth of maximum by Cherenkov light data) and estimated $\rho_\mu(600)/\rho_{\mu+e}(600)$ (the fraction of muons [48–50] by charged and muon component data). Then the data were binned by fraction of muons for three different zenith angles, and in each bin we determined average $\langle X_{\text{max}} \rangle$. Figure 8 shows dependence of X_{max} on fraction of muons for three different zenith angles: 18°, 38°, and 58°. Using the data shown in Fig. 8 and an exponential
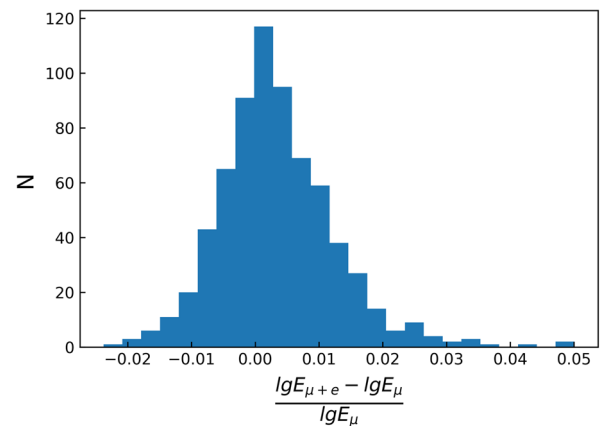

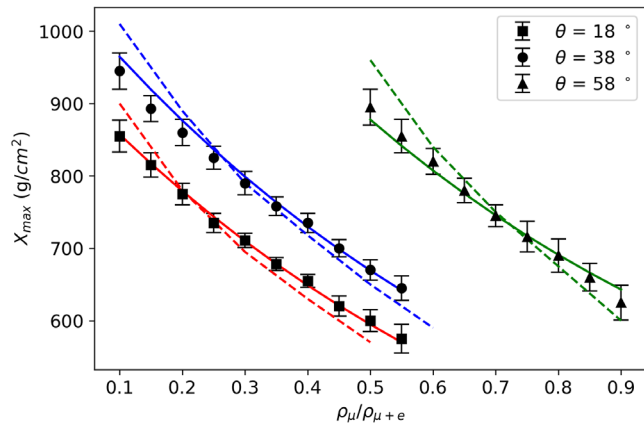FIG. 7. Comparison between energy estimated by muon component and charged component.

FIG. 8. Dependence of depth of maximum of electromagnetic cascade $X_{\max}$ with fraction of muons at the distance of 600 m from the axis $\rho_\mu(600)/\rho_{\mu+e}(600)$. The solid lines are the approximation by Eq. (4) and the dashed lines are the QGSJetII-04 simulations.

function, an empirical relationship was established between $\rho_\mu(600)/\rho_{\mu+e}(600)$ and $X_{\max}$ (7),

$$X_{\max} = A_1 \cdot \exp\left(-\frac{\rho_\mu(600)/\rho_{\mu+e}(600)}{t_1}\right) + y_0. \quad (7)$$

The coefficients A_1, t_1, and y_0 were determined by approximating the experimental data with Eq. (7),

$$
\begin{aligned}
X_{\max} &= (745 + 413 \cdot (\sec\theta - 1)) \\
&\quad \cdot \exp\left(-\frac{\rho_\mu(600)/\rho_{\mu+e}(600)}{-0.818 - 0.037 \cdot (\sec\theta - 1)}\right) \\
&\quad + (172 + 132 \cdot (\sec\theta - 1)).
\end{aligned} \quad (8)
$$

In Fig. 8 the curves show the approximations of the experimental data for each zenith angle according to (8). There is a good agreement between experimental data and

fit. For the first zenith angle $\chi_1^2 = 0.28$, for the second and third, respectively, $\chi_2^2 = 1.86$ and $\chi_3^2 = 1.34$.

Equation (8) was used to calculate $X_{\max}$ in individual showers from the parameter $\rho_\mu(600)/\rho_{\mu+e}(600)$. The total accuracy—statistical and systematic—of determination of $X_{\max}$, according to modeling is $25 \pm 8 \ \mathrm{g \cdot cm^{-2}}$ [49]. Table II shows the data in Fig. 8.

This method allows us to significantly increase the number of showers with estimated $X_{\max}$ in our data. Comparing the annual time for registering muons and Cherenkov light at the Yakutsk array, it is 50–60% and 6–10%, respectively. In addition, this technique does not depend on weather conditions, while the registration of Cherenkov light depends on the transparency of the atmosphere; haze, cloudiness, the presence of the Moon in the sky, the Northern Lights, and other factors.

In addition, Fig. 8 also shows the QGSJetII-04 simulations for zenith angles $\langle\theta\rangle = 18°$, $\langle\theta\rangle = 38°$, and $\langle\theta\rangle = 58°$. The simulations were performed using the CORSIKA [51], with thinning parameter ($t = 10^{-5}$). The simulation took into account the response of a scintillation detector with a threshold of 10 MeV and response uncertainty caused by the registering electronics and taking into account the overlap material (in the case of a muon detector response) [52]. It can be seen from Fig. 8 that there are discrepancies between experimental data and simulations. These discrepancies are possibly associated with experimental errors and model flaws in describing the muon component [53–55]. The details of these discrepancies need further analysis and explanations.

In Fig. 9 the dots show the values of depth of maximum $X_{\max}$ obtained from the fraction of muons $\rho_\mu(600)/\rho_{\mu+e}(600)$ in individual air showers with energies greater than 1 EeV. Further, the array of points was binned with a step $\Delta \lg E = 0.2$, and in each interval, by averaging individual showers, the average values of $\langle X_{\max}\rangle$ were found; these results are shown in Fig. 10(a) with red triangles. An analysis of the data showed that the shift of

TABLE II. $X_{\max}$ and $\rho_\mu/\rho_{\mu+e}$ for different zenith angles.

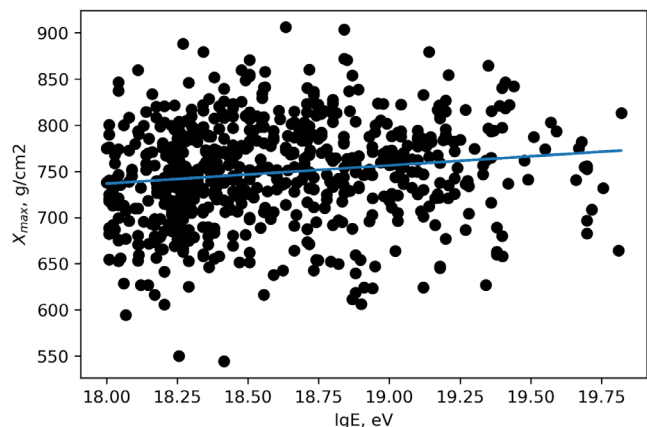| $\langle\theta\rangle = 18°$		$\langle\theta\rangle = 38°$		$\langle\theta\rangle = 58°$	
$\rho_\mu/\rho_{\mu+e}$	$X_{\max} \pm$ stat	$\rho_\mu/\rho_{\mu+e}$	$X_{\max} \pm$ stat	$\rho_\mu/\rho_{\mu+e}$	$X_{\max} \pm$ stat
0.10	855 ± 22	0.10	945 ± 25	0.50	895 ± 25
0.15	815 ± 17	0.15	893 ± 18	0.55	855 ± 23
0.20	775 ± 15	0.20	860 ± 18	0.60	820 ± 18
0.25	735 ± 13	0.25	825 ± 16	0.65	780 ± 17
0.30	711 ± 10	0.30	790 ± 16	0.70	745 ± 15
0.35	678 ± 9	0.35	758 ± 13	0.75	716 ± 21
0.40	655 ± 9	0.40	735 ± 13	0.80	690 ± 23
0.45	620 ± 14	0.45	700 ± 12	0.85	660 ± 19
0.50	600 ± 15	0.50	670 ± 14	0.90	625 ± 24
0.55	575 ± 20	0.55	645 ± 17	⋯	⋯

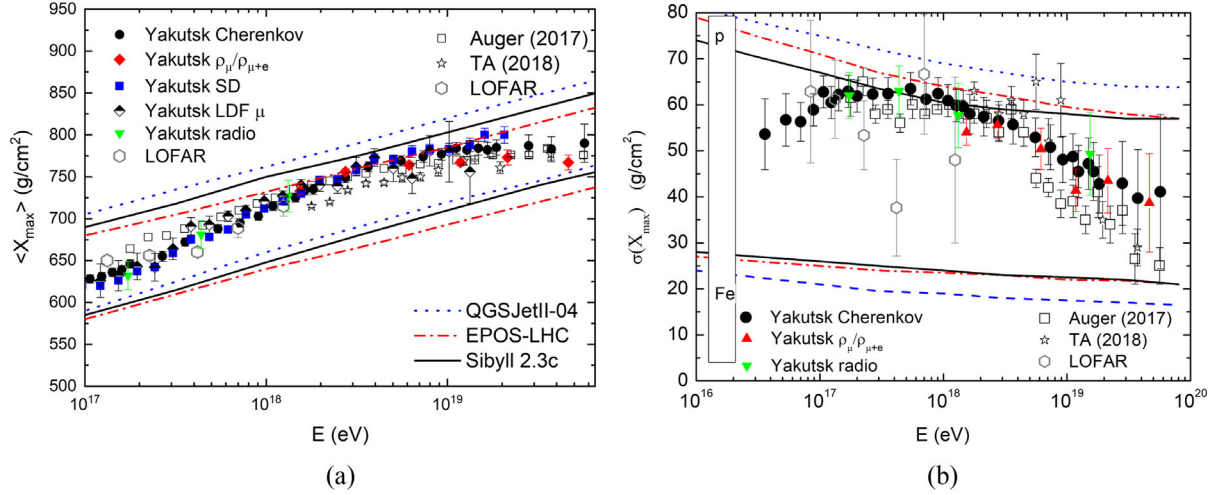FIG. 9. Individual showers with energy greater than 1 EeV.

FIG. 10. (a) dependence of depth of maximum development of air showers X_{max} on energy E_0. It includes data on small and large arrays. Lines show simulations of different models of hadronic interactions for primary proton and iron nucleus; (b) dependence of fluctuations $\sigma(X_{max})$ on energy E_0 and its comparison with other experiments and model calculations.

X_{max} to sea level with increasing energy is insignificant and its elongation rate (E.R.) is equal to 40 ± 6 g·cm^{-2} for one order of magnitude. This is much less than in the energy range 0.1–1 EeV, where E.R. $= 78 \pm 5$ g·cm^{-2} [28]. Most likely, this is due to a change in the mass composition of cosmic rays towards heavier particles; CNO and Fe nuclei. In this respect, it is interesting to consider fluctuations of $\langle X_{max} \rangle$, the magnitude of which directly depends on the atomic weight of the primary particles. The results of this analysis are presented below.

C. Dependence of X_{max} on E_0

Using a sample of showers with energies greater than 5 EeV and muon component data, in each shower, the fraction of muons at a distance of 600 m from the shower axis was determined. The depth of the air shower development X_{max} was determined by Eq. (8). X_{max} data was divided into energy intervals, and the average depth of maximum $\langle X_{max} \rangle$ was determined in each interval. In these intervals, fluctuations in $\sigma(X_{max})_{meas}$ were also calculated. To estimate the physical fluctuations in the development of air showers $\sigma(X_{max})_{phys}$, we used the measurement fluctuations $\sigma(X_{max})_{meas}$ and instrumental fluctuations $\sigma(X_{max})_{app}$. These are fluctuations in the response of the scintillation detector, the accuracy of determining the shower axis, zenith angle, and reconstructing X_{max}, which were obtained by full Monte Carlo simulation of measurements of muons and charged particles at the Yakutsk array [56–59]. A simulation was carried out by QGSJetII-04 model [60] for given energies and zenith angles. The model takes into account the physical fluctuation associated with the fluctuation of the first interaction point and the characteristics of mainly hadronic component and their influence on the final fluctuation of charged particles and

muons at sea level. Next, simulated showers were passed through the Yakutsk array registration system according to geometry of detectors with known signal response dispersion and to the experiment triggering system [61]. Certain position at the array were chosen in order to evaluate the effect of their location on the array plane (center, periphery, perimeter boundary, beyond the perimeter) on the accuracy of air shower characteristics reconstruction. For each known axis location with known characteristics were simulated 100 air showers. After the reconstruction of the air shower characteristics we compared them with simulated showers in order to obtain errors of characteristics estimation, including accuracy of determination of ratio $\rho_\mu(600)/\rho_{\mu+e}(600)$ and then X_{max}. Instrumental error was determined by comparing simulated and reconstructed X_{max}, taking into account the inherent errors according to the equation $\sigma^2(X_{max})_{app} = \sigma^2_{loc} + \sigma^2_\theta + \sigma^2_{\rho_\mu/\rho_{\mu+e}}$, where σ^2_{loc} is the shower axis reconstruction error, σ^2_θ is the zenith angle determination error, and $\sigma^2_{\rho_\mu/\rho_{\mu+e}}$ is the ratio of muon and charged particles flux determination error.

So the average instrumental error at an energy of 10^{18} eV is equal to $\langle \sigma(X_{max})_{app} \rangle = 38$ g/cm^2 and its dependence on energy can be expressed as

$$\langle \sigma(X_{max}) \rangle = (38.5 \pm 5) - (10 \pm 3) \; \lg \frac{E_0}{10^{18}}. \quad (9)$$

Then the physical fluctuation $\sigma^2(X_{max})_{phys}$ is

$$\sigma^2(X_{max})_{phys} = \sigma^2(X_{max})_{meas} - \sigma^2(X_{max})_{app}. \quad (10)$$

Figure 10 shows dependence of $\langle X_{max} \rangle$ on energy and fluctuations of $\sigma\langle X_{max} \rangle$ on energy. Figure 10(a) shows the Yakutsk array data (red triangles) in comparison with

other components: Cherenkov light[28], scintillation detectors, the LDF of the muon component [62,63], and radio emission [36]. In addition, the figure shows the data of the other experiments: Auger [64,65], Telescope Array [14,66], LOFAR [67] and simulations of QGSJetII-04 [60], Sibyll 2.3c [68], EPOS-LHC [69]. The results of the Yakutsk array for X_{max}, obtained for different components, agree with each other within the experimental errors and reflect the uneven course of X_{max} with increasing energy. This is especially evident, starting from an energy of 5 EeV, where the displacement rate X_{max} noticeably decreases. This is not contradicted by the muon data obtained in this work.

The Auger and Telescope Array data are somewhat different from each other, although do not contradict each other within systematic and statistical uncertainty. In paper [70] it is shown that there is a good agreement between the Auger and TA measurements of $\sigma(X_{max})$ up to energies $10^{18.7}$ eV. For greater energies, because of statistical fluctuation, it is more difficult to draw any firm conclusions.

Independent estimations of X_{max} made from measurements of radio emission at the Yakutsk and LOFAR experiments [67] agree with the data obtained in the optical wavelength range and confirm the general behavior of the dependence of X_{max} on energy in the energy range 0.1–1 EeV.

Figure 10(b) shows fluctuations of $\sigma\langle X_{max}\rangle$ on energy of the Yakutsk array and the Auger and Telescope Array. An analysis of the general results shown in Fig. 10(b) indicates the variability of the fluctuations of $\langle X_{max}\rangle$ in a wide range of energies. In the energy range 0.1–1 EeV, the fluctuations reach its maximum value, which corresponds to the light composition of cosmic rays (protons and helium nuclei). Starting with energies of 5–8 EeV, fluctuations gradually decrease, which indicates a heavier composition of cosmic rays.

III. COMPOSITION OF COSMIC RAYS IN THE RANGE OF HIGHEST ENERGIES

The mass composition of cosmic rays $\langle \ln A \rangle$ is estimated by interpolation (11) [17,71].

$$\langle \ln A \rangle = \frac{X_{max}^{exp} - X_{max}^{p}}{X_{max}^{Fe} - X_{max}^{p}} \cdot \ln A_{Fe} \qquad (11)$$

Here, X_{max}^{p} is the depth of maximum development simulated for the proton with QGSJetII-04, X_{max}^{Fe} is for the iron nucleus. X_{max}^{exp} is the depth of maximum development, estimated by muon data [Fig. 10(a)], and $\ln A_{Fe}$ is the natural logarithm of the atomic weight of iron.

The results of the Yakutsk array for $\langle \ln A \rangle$ using muons are shown in Fig. 11 with a red triangle. In addition, there is estimated $\langle \ln A \rangle$ value by other components measured at the Yakutsk array in a wider energy range [Fig. 10(a)] [14,28,65]. It follows from Fig. 11 that the results indicate a sharp decrease in the value of $\langle \ln A \rangle$ in the energy range
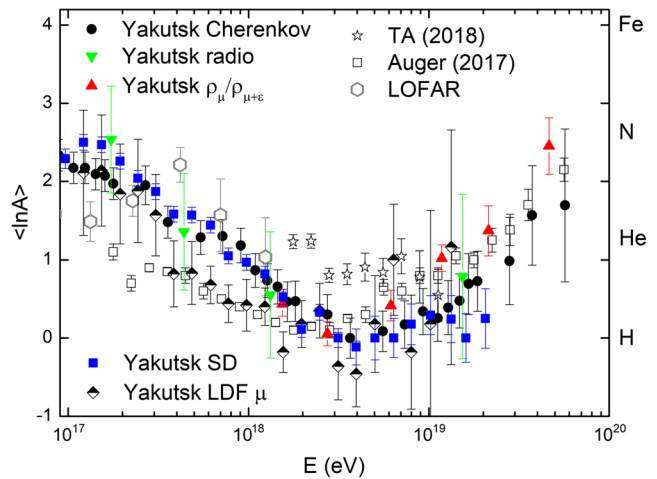

FIG. 11. Mass composition of cosmic rays. The results of the Yakutsk array for $\langle \ln A \rangle$ using muons are shown with a red triangles. Estimation of MC by other components: Yakutsk Cherenkov [28] (dots), Yakutsk radio [36,72] (green triangles), Yakutsk SD [63] (blue squares), and LDF μ [62] (diamonds). Comparison with other experiments: LOFAR [67], TA [73], and Auger [65].

3–5 EeV, which means light mass composition—protons and helium nuclei in cosmic rays in this energy range. In the energy range of 5 EeV, the $\langle \ln A \rangle$ value starts to increase, which indicates an increase in the mass composition of the primary particles. For comparison, Fig. 11 shows the data from the Telescope Array [14], Auger [65], and LOFAR [67] experiments. There is a significant scatter in the data; Auger data in the range of 0.1–1 EeV indicate a composition consisting of protons and helium nuclei, while data from the Yakutsk and LOFAR experiments indicate a composition consisting of helium and CNO nuclei. The results of the Telescope Array in the energy range of 1–10 EeV do not agree with the data of the Yakutsk and the Auger. Only in the region $E_0 \geq 5$ EeV, the results of all experiments agree with each other within the experimental errors and indicate a general tendency for an increase of heavy nuclei in the flux of cosmic rays. The trend is shown by results obtained from the muon component of the air showers. Uncertainty associated with lack of knowledge of the real model of air shower development (by the example of muons), as can be seen from Fig. 11, cannot influence the conclusion about an increase in heavy nuclei in the cosmic ray flux, starting from energies of 30 EeV.

IV. CONCLUSION

In this work, depth of the air shower maximum development X_{max}, based on the parameter $\rho_{\mu}(600)/\rho_{\mu+e}(600)$ in showers with energies greater than 5 EeV, was estimated independently of the model of hadronic interaction. Average values of $\langle X_{max}\rangle$ and their dependence on energy were found from air showers data narrow energy intervals [Fig. 10(a)]. In the same energy ranges, fluctuations in σ

(X_{max}) were estimated [Fig. 10(b)]. Comparison of the experimental data X_{max}, σ (X_{max}) with the calculations of the QGSJetII-04, EPOS-LHS, Sibyll 2.3c models for the primary proton and the iron nucleus indicates that mass composition of cosmic rays changes at energies greater than 5 EeV (Fig. 11).

According to the data of the Yakutsk and other air shower experiments, it can be concluded that the composition of cosmic rays consists of a mixture of light nuclei in the energy range of 5–10 EeV [Fig. 10(b) and Fig. 11]. This is also indicated by the rapid shift of X_{max} at the sea level E.R. = 63 ± 6 g · cm^{-2} [Fig. 10(a)] [28], which is typical for a mixture of light nuclei (protons and helium nuclei).

For energies greater than 30 EeV, as can be seen from Fig. 11, the mass composition of cosmic rays begins to change towards heavier elements (CNO nuclei and iron).

Results from independent radio emission measurements of the Yakutsk and LOFAR experiments [36,67] complement this conclusion.

It should be noted that the mass composition of cosmic rays, determined using modern models of hadronic interactions is preliminary. Since the models do not fully reflect the real development of extensive air showers in the atmosphere, for example, in terms of muons. Discussions are currently underway on this issue [53–55].

ACKNOWLEDGMENTS

[1] V. L. Ginzburg, *Modern Astrophysics* (in Russian) (Atom, Moscow, 1970), p. 192.

[2] V. L. Ginzburg, What problems of physics and astrophysics seem now to be especially important and interesting (Thirty years later, already on the verge of XXI century)?, Phys. Usp. **42,** 353 (1999).

[3] G. Gelmini, O. Kalashev, and D. Semikoz, GZK photons as ultra-high-energy cosmic rays, J. Theor. Phys. **106,** 1061 (2008).

[4] P. Bhattacharjee and G. Sigl, Origin and propagation of extremely high energy cosmic rays, Phys. Rep. **327,** 109 (2000).

[5] F. Halzen and D. Hooper, High-energy neutrino astronomy: The cosmic ray connection, Rep. Prog. Phys. **65,** 1025 (2002).

[6] J.-T. Li, E. Hodges-Kluck, Y. Stein, J. Bregman, J. Irwin, and R.-J. Dettmar, Detection of non-thermal hard X-ray emission from the "Fermi bubble" in an external galaxy, Astrophys. J. **873,** 27 (2019).

[7] K. Mannheim, R. J. Protheroe, and J. P. Rachen, Cosmic ray bound for models of extragalactic neutrino production, Phys. Rev. D **63,** 023003 (2000).

[8] H. Kang, D. Ryu, and T. Jones, Cluster accretion shocks as possible acceleration sites for ultra–high-energy protons below the Greisen cutoff, Astrophys. J. **456,** 422 (1996).

[9] J. Rachen and P. Biermann, Extragalactic ultra-high energy cosmic-rays—Part one—Contribution from hot spots in Fr-II radio galaxies, Astron. Astrophys. **272,** 161 (1993).

[10] E. Waxman, Cosmological Gamma-Ray Bursts and the Highest Energy Cosmic Rays, Phys. Rev. Lett. **75,** 386 (1995).

[11] E. Berezhko, Cosmic rays from active galactic nuclei, Astrophys. J. **684,** L69 (2008).

[12] G. N. Kichigin, The surfatron acceleration of cosmic rays in the galactic plasma, J. Exp. Theor. Phys. **92,** 895 (2001).

[13] S. Knurenko, Z. Petrov, and I. Petrov, Second knee on the spectrum of cosmic ray at energies ~10^{17} eV by long-term observations of small Cherenkov EAS array, Phys. At. Nucl. **82,** 732 (2019).

[14] R. Abbasi, M. Abe, T. Abu-Zayyad, M. Allen, R. Azuma, E. Barcikowski, J. Belz, D. Bergman, S. Blake, R. Cady *et al.*, The cosmic-ray energy spectrum between 2 PeV and 2 EeV observed with the tale detector in monocular mode, Astrophys. J. **865,** 74 (2018).

[15] R. Abbasi, M. Abe, T. Abu-Zayyad, M. Allen, R. Azuma, E. Barcikowski, J. Belz, D. Bergman, S. Blake, R. Cady *et al.*, The energy spectrum of cosmic rays above 1017.2 eV measured by the fluorescence detectors of the telescope array experiment in seven years, Astropart. Phys. **80,** 131 (2016).

[16] R. Abbasi, M. Abe, T. Abu-Zayyad, M. Allen, R. Azuma, E. Barcikowski, J. Belz, D. Bergman, S. Blake, R. Cady *et al.*, The cosmic-ray composition between 2 PeV and 2 EeV observed with the tale detector in monocular mode, Astrophys. J. **909,** 178A (2021).

[17] E. Berezhko, S. Knurenko, and L. Ksenofontov, Composition of cosmic rays at ultra high energies, Astropart. Phys. **36,** 31 (2012).

[18] S. Buitink, A. Corstanje, H. Falcke *et al.*, A large light-mass component of cosmic rays at $10^{17} - 10^{17.5}$ electronvolts from radio observations, Nature (London) **531,** 70 (2016).

[19] K.-H. Kampert and M. Unger, Measurements of the cosmic ray composition with air shower experiments, Astropart. Phys. **35,** 660 (2012).

[20] I. Ivanenko, I. Rapoport, and V. Shestoperov, *Energy Spectrum and Charge Composition: Cosmic Rays with Energy 2–100 TeV by Results of Satellite "Cosmos-1713"* (Skobeltsyn Institute of Nuclear physics, Moscow, 1988), p. 26.

[21] N. Grigorov, Is the difference in the spectra of protons and heavier nuclei in the high-energy region a myth or reality?, Kosm. Issled. **33,** 339 (1995).

[22] V. I. Zatsepin, M. I. Panasyuk, A. D. Panov, and N. V. Sokolskaya, Direct measurements of galactic cosmic-ray

energy spectra and elemental composition, Moscow Univ. Phys. Bull. **6,** 493 (2012).

[23] O. Adriani, G. C. Barbarino, G. A. Bazilevskaya, R. Bellotti, M. Boezio, E. A. Bogomolov, L. Bonechi, M. Bongi, V. Bonvicini, S. Borisov *et al.*, PAMELA measurements of cosmic-ray proton and helium spectra, Science **332,** 69 (2011).

[24] M. Aguilar, D. Aisa, B. Alpat, A. Alvino, G. Ambrosi, K. Andeen, L. Arruda, N. Attig, P. Azzarello, A. Bachlechner *et al.* (AMS Collaboration), Precision Measurement of the Proton Flux in Primary Cosmic Rays from Rigidity 1 GV to 1.8 TV with the Alpha Magnetic Spectrometer on the International Space Station, Phys. Rev. Lett. **114,** 171103 (2015).

[25] D. M. Green and E. A. Hays, Measurement of the cosmic-ray proton spectrum with the Fermi large area telescope, Proc. Sci. 301 (**2018**) 159.

[26] A. Panov *et al.*, Energy spectra of abundant nuclei of primary cosmic rays from the data of atic-2 experiment: Final results, Bull. Russ. Acad. Sci. **73,** 564 (2009).

[27] E. Seo *et al.*, CREAM: 70 days of flight from 2 launches in Antarctica, Adv. Space Res. **42,** 1656 (2008).

[28] S. P. Knurenko and I. S. Petrov, Mass composition of cosmic rays above 0.1 EeV by the Yakutsk array data, Adv. Space Res. **64,** 2570 (2019).

[29] A. Aab, P. Abreu, M. Aglietta *et al.*, The pierre auger cosmic ray observatory, Nucl. Instrum. Methods Phys. Res., Sect. A **798,** 172 (2015).

[30] T. Abu-Zayyad, R. Aida, M. Allen, R. Anderson, R. Azuma, E. Barcikowski, J. Belz, D. Bergman, S. Blake, R. Cady *et al.*, The surface detector array of the Telescope array experiment, Nucl. Instrum. Methods Phys. Res., Sect. A **689,** 87 (2012).

[31] S. Knurenko and A. Sabourov, The depth of maximum shower development and its fluctuations: Cosmic ray mass composition at $E_0 \geq 10^{17}$ eV, Astrophys. Space Sci. Trans. **7,** 251 (2011).

[32] S. P. Knurenko and I. S. Petrov, Mass composition of cosmic rays determined by the muon fraction with $\varepsilon_{thr} \geq 1$ GeV in air showers with energy greater than 5 EeV, Phys. Rev. D **102,** 023036 (2020).

[33] J. Abraham, P. Abreu, M. Aglietta *et al.*, Trigger and aperture of the surface detector array of the Pierre Auger Observatory, Nucl. Instrum. Methods Phys. Res., Sect. A **613,** 29 (2010).

[34] A. Atrashkevich, N. Kalmykov, and G. Christiansen, On the possibility of studying the chemical composition of primary cosmic radiation at energies of the order and more than 10^{17} eV, ZhETF Pisma Redaktsiiu **33,** 236 (1981).

[35] G. Khristiansen, Y. Fomin, N. Kalmykov, G. Kulikov, M. Motova, S. Ostapchenko, V. Sulakov, and A. Trubitsyn, Primary cosmic ray mass composition at energies $10^{15} - 10^{17}$ eV as measured by the MSU EAS array, Astropart. Phys. **2,** 127 (1994).

[36] S. Knurenko, Z. Petrov, and I. Petrov, Radio emission of air showers with extremely high energy measured by the Yakutsk radio array, Nucl. Instrum. Methods Phys. Res., Sect. A **866,** 230 (2017).

[37] S. Thoudam, J. Rachen, A. van Vliet, A. Achterberg, S. Buitink, H. Falcke, and J. Hörandel, Cosmic-ray energy spectrum and composition up to the ankle: The case for a second galactic component, Astron. Astrophys. **595,** A33 (2016).

[38] M. Glasmacher, M. A. Catanese, M. Chantell *et al.*, The cosmic ray composition between 10^{14} and 10^{16} eV, Astropart. Phys. **12,** 1 (1999).

[39] N. Chiba, K. Hashimoto, N. Hayashida *et al.*, Akeno Giant Air Shower Array (AGASA) covering 100 km^2 area, Nucl. Instrum. Methods Phys. Res., Sect. A **311,** 338 (1992).

[40] W. Apel, J. Arteaga, A. Badea *et al.*, The KASCADE-Grande experiment, Nucl. Instrum. Methods Phys. Res., Sect. A **620,** 202 (2010).

[41] A. Aab, P. Abreu, M. Aglietta, E. J. Ahn, I. Al Samarai, I. F. M. Albuquerque, I. Allekotte, P. Allison, A. Almela, J. Alvarez Castillo, J. Alvarez-Muñiz, R. Alves Batista, M. Ambrosio, A. Aminaei, and L. Anchordoqui *et al.*, The Pierre Auger observatory upgrade—Preliminary design report (2016).

[42] V. Artamonov, B. Afanasyev, A. Glushkov *et al.*, Status and prospects of the Yakutsk complex array of EAS, Bull. Russ. Acad. Sci. **58,** 98 (1994).

[43] G. Garipov, V. Grigoryev, N. Efremov *et al.*, The Cherenkov track detector consisting of the Yakutsk complex EAS array, *Proceeding of 27th ICRC, Hamburg, Germany* (2001), Vol. 2, p. 885.

[44] Y. Egorov, Z. Petrov, and S. Knurenko, Cherenkov differential detector at the Yakutsk extensive air shower array, Proc. Sci. 301 (**2018**) 462.

[45] D. D. Krasilnikov, S. Knurenko, V. A. Kolosov *et al.*, The spectrum of ultra-high energy EASs, in *Cosmic Rays with Energy Above 1017 eV* (1983), p. 117.

[46] S. Knurenko, A. Makarov, M. Pravdin, and A. Sabourov, The relation between charged particles and muons with threshold energy 1 GeV in extensive air showers registered at the Yakutsk EAS array, *Proceeding of XVI ISVHECRI 2010, Batavia, USA* (2010), p. C13.

[47] S. Knurenko, A. Makarov, M. Pravdin, and A. Sabourov, Portion of muons with a threshold energy above 1 GeV in extensive air showers with ultra-high energies, according to the Yakutsk EAS array data, Bull. Russ. Acad. Sci. Phys. **75,** 291 (2011).

[48] M. Dyakonov, S. Knurenko, V. Kolosov, D. D. Krasilnikov, F. F. Lischenyuk, I. E Sleptsov, and S. I. Nikolsky, The use of cherenkov detectors at the Yakutsk cosmic ray extensive air shower array, Nucl. Instrum. Methods Phys. Res., Sect. A **248,** 224 (1986).

[49] S. Knurenko, V. Kolosov, and Z. Petrov, *Proceeding of 27-th ICRC, Hamburg (Germany)* (2001), Vol. 1, p. 157.

[50] A. Kochnev, Adaptive method of linear equation system solutions in geophysics, *Proceeding of 'Use of PC in Control Problems', Krasnoyarsk (USSR)* (1985), 62.

[51] D. Heck, J. Knapp, J. N. Capdevielle, G. Schatz, and T. Thouw, *CORSIKA: A Monte Carlo code to Simulate Extensive Air Showers* (Forschungszentrum Karlsruhe GmbH, Karlsruhe, Germany, 1998).

[52] A. Sabourov, Spatial distribution of EAS particles with energies above 10^{17} eV according to the data of the Yakutsk array, dissertation SB RAS, Moscow, INR, 146, 2017.

[53] H. Dembinski, J. Arteaga-Velázquez, L. Cazon, R. Conceição, J. Gonzalez, Y. Itow *et al.*, Hadronic interaction

properties with air showers, EPJ Web Conf. **210,** 02004 (2019).

[54] L. Cazon *et al.*, Working group report on the combined analysis of muon density measurements from eight air shower experiments, Proc. Sci. 358 (**2021**) 214.

[55] J. Espadanal, L. Cazon, and R. Conceição, Sensitivity of EAS measurements to the energy spectrum of muons, Astropart. Phys. **86,** 32 (2017).

[56] A. Ivanov, S. Knurenko, and I. Sleptsov, Measuring extensive air showers with Cherenkov light detectors of the Yakutsk array: The energy spectrum of cosmic rays, New J. Phys. **11,** 065008 (2009).

[57] A. Ivanov, Numerical study of extensive air showers of ultrahigh energy cosmic rays, dissertation, Yakutsk, SB RAS, 228, 2005.

[58] M. Dyakonov, A. Ivanov, S. Knurenko *et al.*, Simulation of measurements at the Yakutsk complex EAS array, *Proceeding of 17 ICRC. Paris (France)* (1981), Vol. 6, p. 78.

[59] M. Dyakonov, A. Ivanov, S. Knurenko *et al.*, *Electromagnetic Cascade Profiles and Fluctuations of EAS Lateral Distribution* (Yadernaya Fizika SB AS USSR, Yakutsk, 1983), pp. 34–47.

[60] S. Ostapchenko, Monte Carlo treatment of hadronic interactions in enhanced Pomeron scheme: I. QGSJET-II model, Phys. Rev. D **83,** 014018 (2011).

[61] S. Knurenko, Dissertation, Yakutsk, SB RAS, 168, 2003.

[62] A. Glushkov and A. Sabourov, Mass composition of cosmic rays with energies above 10^{17} eV according to the data from the muon detectors of the Yakutsk EAS array, JETP Lett. **109,** 559 (2019).

[63] A. Glushkov and A. Saburov, Estimation of the cosmic ray mass composition at energy above 10^{17} eV according to scintillation detectors of the Yakutsk array, Phys. At. Nucl. **82,** 674 (2020).

[64] A. Aab, P. Abreu, M. Aglietta, E. Ahn, I. A. Samarai, I. Albuquerque, I. Allekotte, J. Allen, P. Allison, A. Almela *et al.*, Depth of maximum of air-shower profiles at the Pierre Auger collaboration. II. Composition implications, Phys. Rev. D **90,** 122006 (2014).

[65] J. Bellido, A. Aab, P. Abreu, M. Aglietta, I. Albuquerque, J. Albury, I. Allekotte, A. Almela, J. A. Castillo, J. Alvarez-Muñiz, G. Anastasi *et al.*, Depth of maximum of air shower profiles at the Pierre Auger Observatory: Measurements above $10^{17.2}$ and composition implications, Proc. Sci. 301 (**2018**) 506.

[66] R. Abbasi, M. Abe, T. Abu-Zayyad, M. Allen, R. Azuma, E. Barcikowski, J. Belz, D. Bergman, S. Blake, R. Cady *et al.*, Study of ultra-high energy cosmic ray composition using Telescope array middle drum detector and surface array in hybrid mode, Astropart. Phys. **64,** 49 (2015).

[67] A. Corstanje, S. Buitink, H. Falcke, B. Hare, J. Hörandel, T. Huege *et al.*, Depth of shower maximum and mass composition of cosmic rays from 50 PeV to 2 EeV measured with the LOFAR radio telescope, Phys. Rev. D **103,** 102006 (2021).

[68] F. Riehn, R. Engel, A. Fedynitch, T. Gaisser, and T. Stanev, A new version of the event generator Sibyll, Proc. Sci. 236 (**2015**) 558.

[69] T. Pierog, I. Karpenko, J. M. Katzy, E. Yatsenko, and K. Werner, EPOS LHC: Test of collective hadronization with data measured at the CERN large hadron collider, Phys. Rev. C **92,** 034906 (2015).

[70] A. Yushkov, J. Bellido, W. H. V. de Souza, D. Ikeda, P. Sokolsky, Y. Tsunesada, M. Unger *et al.*, Depth of maximum of air-shower profiles: Testing the compatibility of measurements performed at the Pierre Auger Observatory and the Telescope array experiment, EPJ Web Conf. **107,** 01009 (2019).

[71] J. Hörandel, A review of experimental results at the knee, J. Phys. Conf. Ser. **47,** 41 (2006).

[72] S. Knurenko and I. Petrov, Characteristics of air showers with energy more than 10^{17} eV reconstructed by the Yakutsk array radio emission measurements, EPJ Web Conf. **208,** 08017 (2019).

[73] R. Abbasi, M. Abe, T. Abu-Zayyad, M. Allen, R. Azuma, E. Barcikowski, J. Belz, D. Bergman, S. Blake, R. Cady *et al.*, Mass composition of ultrahigh-energy cosmic rays with the telescope array surface detector data, Phys. Rev. D **99,** 022002 (2019).